Heterogeneously integrated III-V/silicon distributed feedback lasers

S. Keyvaninia,[1,2,*] S. Verstuyft,[1,2] L. Van Landschoot,[1,2] F. Lelarge,[3] G.-H. Duan,[3] S. Messaoudene,[4] J. M. Fedeli,[4] T. De Vries,[5] B. Smalbrugge,[5] E. J. Geluk,[5] J. Bolk,[5] M. Smit,[5] G. Morthier,[1,2] D. Van Thourhout,[1,2] and G. Roelkens[1,2,5]

[1]*Photonics Research Group, INTEC, Ghent University-IMEC, Sint-Pietersnieuwstraat 41, B-9000 Ghent, Belgium*

[2]*Center for Nano- and Biophotonics (NB-Photonics), Ghent, Belgium*

[3]*III-V Lab, a joint laboratory of 'Alcatel-Lucent Bell Labs France,' 'Thales Research and Technology' and 'CEA Leti,' Campus Polytechnique, 1, Avenue A. Fresnel, 91767 Palaiseau cedex, France*

[4]*'CEA Leti,' LETI, Minatec, 17 rue des Martyrs, F-38054 GRENOBLE cedex 9, France*

[5]*Photonic Integration Group, Eindhoven University of Technology, Den Dolech 2, Eindhoven, The Netherlands*

**Corresponding author: shahram.keyvaninia@intec.ugent.be*

Received July 17, 2013; revised October 10, 2013; accepted October 21, 2013; posted October 21, 2013 (Doc. ID 194029); published December 12, 2013

Heterogeneously integrated III-V-on-silicon second-order distributed feedback lasers utilizing an ultra-thin DVS-BCB die-to-wafer bonding process are reported. A novel DFB laser design exploiting high confinement in the active waveguide is demonstrated. A 14 mW single-facet output power coupled to a silicon waveguide, 50 dB side-mode suppression ratio and continuous wave operation up to 60°C around 1550 nm is obtained. © 2013 Optical Society of America

OCIS codes: (130.0250) Optoelectronics; (250.5300) Photonic integrated circuits; (140.3490) Lasers, distributed-feedback.

http://dx.doi.org/10.1364/OL.38.005434

Silicon photonics is emerging as an important platform for the realization of high-speed optical transceivers. This is related to the fact that the silicon waveguide circuits, comprising ultra-compact passive waveguide circuitry, high-speed optical modulators, and germanium photodetectors, can be fabricated using complementary metal-oxide-semiconductor (CMOS) fabrication technology in large volumes and at low cost. State-of-the-art passive waveguide circuits [1], low power-consumption resonant modulators [2], and high-speed photodetectors [3] are available on this platform and are accessible through multi-project wafer services. However, the integration of a coherent light source on the silicon platform remains an issue. While electrically driven germanium laser sources have been demonstrated [4], the performance of these devices is still far inferior to what can be achieved using InP-based III-V semiconductors. III-V semiconductor layer stacks can be heterogeneously integrated onto the silicon waveguide circuit using a wafer-bonding technique followed by InP substrate removal, which provides a route toward wafer-scale processing of these III-V epitaxial layers, lithographically aligned to the underlying waveguide circuit. In recent years, several device demonstrations were made on this III-V/silicon platform [5], both using a molecular [6] and adhesive bonding approach [7,8]. In this Letter, we describe the realization of single wavelength 1550 nm distributed feedback (DFB) lasers coupled to a 220 nm thick silicon waveguide layer, with single-facet waveguide-coupled output powers of 14 mW, a side-mode-suppression ratio (SMSR) better than 50 dB and a laser linewidth of 1 MHz. The coupling to a 220 nm silicon waveguide circuit will allow in a later stage to co-integrate high-speed devices such as modulators and photodetectors with the single-wavelength lasers using the available silicon photonics platform technology. The DFB laser structures reported in this Letter are based on quarter-wave shifted second-order gratings with a Bragg wavelength around 1550 nm.

While previously III-V on silicon DFB lasers have been demonstrated in literature [6,9,10], where the optical mode is predominantly confined to the silicon waveguide layer (typically using a >500 nm thick silicon waveguide layer incorporating a shallow grating), in our design the optical mode is strongly confined to the active III-V waveguide layer, as shown in Fig. 2(a). This has several important implications: first the modal gain in these devices is high. The confinement factor per quantum well is almost 2%, which is more than three times higher than in our previous device demonstration [10]. Second, the grating coupling constant κ is not critically dependent on the silicon grating etch depth (where in our previously reported hybrid silicon DFB laser a 5 nm variation in grating etch depth had a large impact on the grating coupling constant [10]), as will be discussed later. Moreover, this laser geometry can be readily implemented on silicon photonic integrated circuits offered by multi-project wafer services using standard 400 nm/220 nm silicon device layer thicknesses. The 3D layout of the laser cavity is depicted in Fig. 1(a), while a longitudinal cross section of the laser geometry is shown in Fig. 1(b). The gratings are defined in a 400 nm thick silicon waveguide layer by a 180 nm deep dry etch, using 193 nm deep UV lithography. The III-V epitaxial layer stack that is used consists of a 200 nm thick n-InP contact layer, two 100 nm thick InGaAsP separate confinement heterostructure layers (bandgap wavelength 1.17 μm), six InGaAsP quantum wells (6 nm thick, emission wavelength 1.55 μm) surrounded by InGaAsP barriers, a 1.5 μm thick p-InP top cladding, and a 100 nm p^{++} InGaAs contact layer. The use of a 400 nm thick silicon waveguide layer in the laser section simplifies the optical coupling between the III-V laser mode (which is completely confined

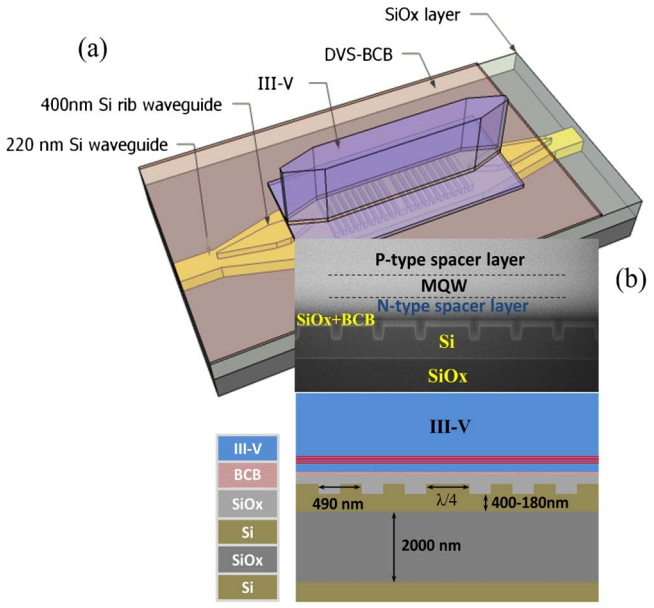

Fig. 1. III-V/Si DFB laser design. (a) Three-dimensional view on the III-V-on-silicon DFB laser. (b) Schematic longitudinal cross section of the laser structure and SEM picture of the actual device.

to the III-V mesa and which evanescently feels the silicon grating) and the silicon waveguide layer, compared to the case of direct coupling to a 220 nm thick device layer. This optical coupling is realized using a III-V/silicon spot-size converter structure defined by tapering both the III-V and silicon waveguide as shown in Fig. 2(a), similar to the structure used in [7,8]. The III-V taper is a piecewise linear taper that quickly tapers (Taper I, $L = 35$ μm) from a 3 μm mesa width to an 0.9 μm wide waveguide width after which a slower adiabatic taper (Taper II, $L = 150$ μm) is implemented by tapering both the III-V and silicon waveguide structure. Using a 400 nm thick silicon waveguide relaxes the requirements on the III-V taper tip width: a width of 500 nm is sufficient to achieve a high-efficiency, low-reflection power transfer from the III-V laser mesa to the silicon waveguide as illustrated by the simulation results in Fig. 2(b). Since the III-V spot-size converter consists of the same active region as the laser, also this spot-size converter is electrically pumped, even though it lies outside the laser cavity. Compared to our previous work [7,8], where the taper structure was implemented inside the laser cavity, in the present device this is no longer the case, implying that the taper structure has no impact on the internal loss (and hence the threshold current density) of the laser cavity. After the laser emission is coupled to the 400 nm thick silicon waveguide layer, a second spot-size converter ($L = 30$ μm) is used to couple to a 220 nm strip waveguide. Quarter-wave shifted second-order DFB gratings with a period of 480 and 490 nm and a duty cycle of 25% were studied. Since the evanescent tail of the laser mode is interacting with the silicon grating, the actual grating coupling strength depends on the III-V/silicon spacing. It is not critically dependent on the shallow silicon grating etch depth as used in classical hybrid DFB lasers [6,9,10], where a 5 nm etch depth variation has a substantial impact on the grating coupling strength.

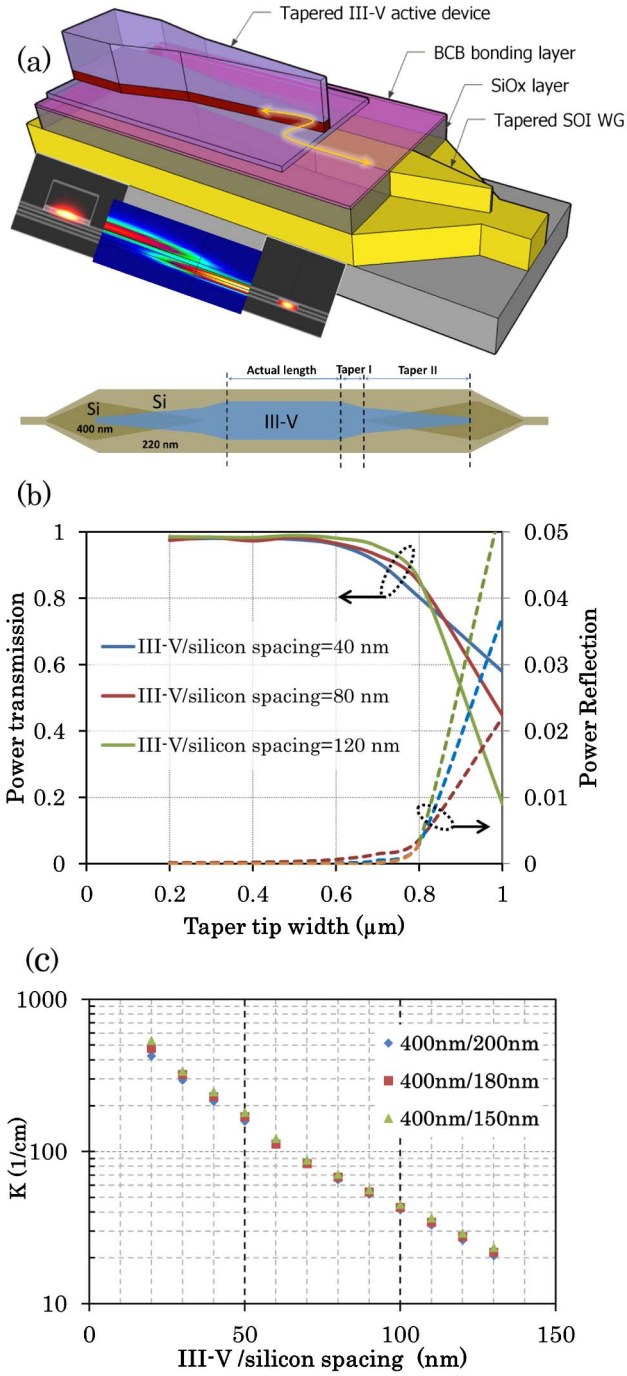

Fig. 2. (a) Spot-size converter structure used in this work. (b) Simulated power transmission and reflection at the spot-size converter taper tip as a function of III-V taper tip width. (c) Grating coupling strength as a function of III-V/silicon spacing and silicon grating etch depth (200, 180, 150 nm) for the second-order grating structure (490 nm period, 25% duty cycle) used in this work.

This grating coupling strength is illustrated in Fig. 2(c) as a function of III-V/silicon spacing and silicon grating etch depth. Given the good uniformity and reproducibility of the adhesive bonding process (±5 nm bonding layer thickness variation is obtained [11]), a reasonable control of the grating-coupling constant between 30 and 40 cm^{-1} can be achieved. Such a variation leads in the current device design to a variation of the drive current to obtain 10 mW output power at 20°C of less than 5%.

The silicon device wafer fabrication is carried out in a CMOS pilot line on 8 in. SOI wafers. The process starts with the etching of a 400 nm silicon device layer on a 2 μm SiO_2 buried oxide layer. In a first etch step, 180 nm deep gratings are etched together with the silicon rib waveguides used in the spot-size converter structure. In a second etch step, 50 nm deep structures are etched in the exposed 220 nm thick silicon device layer in order to realize fiber-to-chip grating couplers.

In a final step, a 220 nm deep etch is used to define the silicon strip waveguides and the transition to the 400 nm device layer. After device etching, the wafer is covered with thick SiO_2, after which chemical mechanical polishing is used to planarize the wafer in combination with wet chemical etching in buffered HF to etch back the SiO_2 leaving 75 nm SiO_2 on top of the silicon waveguide. This way, a quasi-planar wafer surface is obtained. The semiconductor laser material is then bonded to the silicon waveguide circuit using an adhesive die-to-wafer bonding process with a 35 nm thick divinyl-bis-benzocyclobutene (DVS-BCB) adhesive bonding layer. Using such a process, the surface-quality requirements on the III-V and silicon surfaces are relaxed, compared to molecular bonding, resulting in a high bonding yield. This bonding process is described in detail in [11]. While in the used process flow wafer-scale variations of the nominally 75 nm SiO_2 thickness can be expected, much smaller variations can be obtained by using chemical mechanical polishing down to the silicon device layer, after which a 75 nm SiO_2 layer can be accurately deposited using chemical vapor deposition techniques. The 110 nm III-V silicon spacing layer results in a theoretical grating coupling strength of 35 cm^{-1} as can be seen in Fig. 2(c). After bonding, the InP growth substrate is removed, and the III-V laser mesa is defined. In this device demonstration, the III-V mesa and spot-size converter are defined through wet etching, using HCl and H_2O:H_2SO_4:H_2O_2 for the InP and InGaAs/InGaAsP layers, respectively. This wet-etching technique allowed creating undercut structures in the spot-size converter, which again relaxed the lithography requirements in the definition of the III-V spot-size converter, which was realized using 300 nm UV contact lithography. A scanning electron microscope picture of the reverse trapezoidal III-V spot-size converter taper tip is shown in Fig. 3.

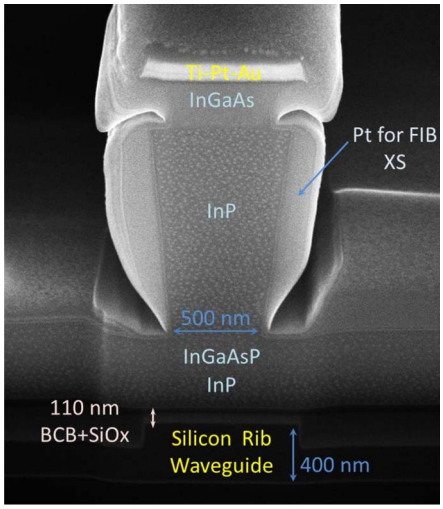

Fig. 3. Scanning electron microscope image of the III-V spot-size converter taper tip illustrating the 500 nm taper tip width close to the active core of the III-V waveguide.

Laser characterization was carried out by collecting the laser emission in a standard single mode fiber using integrated silicon fiber-to-chip grating coupler structures. The coupling efficiency of these grating couplers was characterized on separate structures and used to determine the optical power coupled to the 220 nm silicon strip waveguides. The L–I–V curves of the fabricated laser structures were measured both at room temperature and at elevated temperature. The results for a second-order grating DFB laser (with a period of 490 nm and a device length—not including the spot-size converter—of 680 μm) are shown in Fig. 4. For the given laser structure, a coupling strength κL of 2.4 is obtained. Theoretically, this results in a threshold modal gain excluding internal losses of 15 cm^{-1} ($\Gamma g_{th} - \alpha$ with Γ the optical mode confinement factor in the multi-quantum-well region, g_{th} the material threshold gain, and α the total internal loss—absorption and diffraction losses—per unit length in the laser cavity). Based on this value and on the results obtained on the Fabry–Perot laser reported in [12] using the same epitaxial layer stack, a threshold current density of 1.59 kA/cm^2 is expected, which corresponds reasonably well with the measured threshold current of 35 mA (1.72 kA/cm^2) at 20°C. The characteristic temperature T_0 of the laser is 47 K. The (single-sided) slope efficiency of the laser is 0.135 W/A at 20°C. Based on this experimental slope efficiency, an

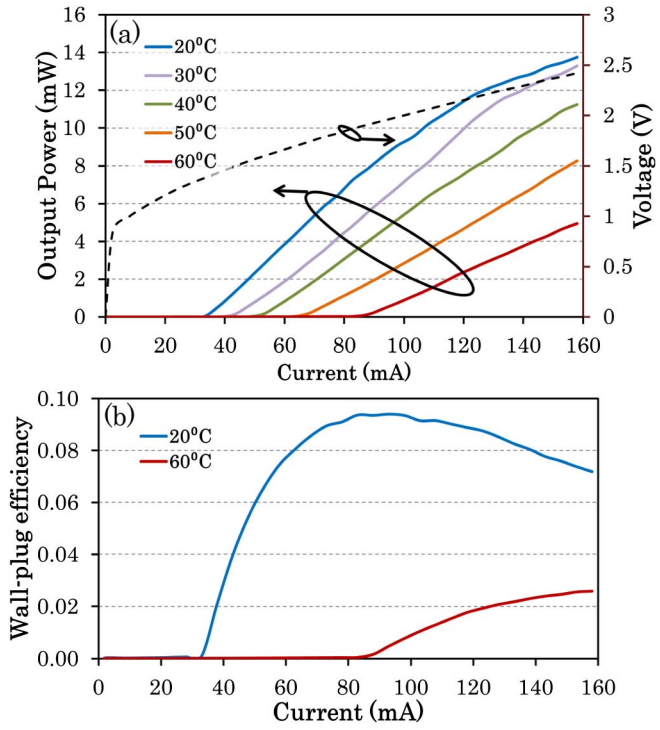

Fig. 4. (a) L–I–V curves at different temperatures for a 490 nm period second-order DFB laser (single facet output power). (b) Wall-plug efficiency of the laser (not considering the thermo-electric cooler) as a function of laser drive current at 20°C and 60°C, taking into account the output power from both facets.

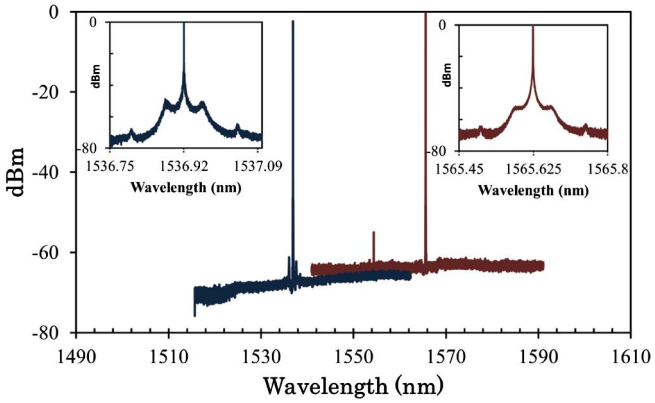

Fig. 5. Spectral characteristics of two second-order DFB lasers (480 nm period and 490 nm period), illustrating single-mode emission. The insets show the high-resolution spectra.

internal loss of 15 cm^{-1} can be derived, since the slope efficiency of the symmetric DFB laser is given by

$$\eta = \frac{1}{2}\frac{h\nu}{q}\eta_i \frac{\Gamma g_{\text{th}} - \alpha}{\Gamma g_{\text{th}}} T\beta, \tag{1}$$

with η_i the injection efficiency (assumed 0.9), $h\nu/q = 0.8$ mW/mA at 1550 nm, T the taper transmission (assumed to be 90% irrespective of the injection current) and β the ratio between the DFB laser active area and the total area of the device, including the taper structures ($\beta = 0.84$ in this work). At 160 mA drive current an optical output power of 14 mW coupled into the silicon waveguide is obtained. At 60°C, 4 mW optical output power is still obtained. The series resistance of the laser was 7.5 Ω. Figure 5 shows the laser spectrum for two second-order DFB lasers with a grating period of 480 and 490 nm, respectively, (both a broad wavelength scan and a narrow wavelength scan, measured with a 15 MHz resolution spectrum analyzer) at a bias current of 100 mA (3 I_{th}) for both lasers, showing clearly single-mode operation with a SMSR of more than 50 dB. Single-mode operation was observed over the whole laser drive current range, indicating that no significant spatial hole burning occurs. Finally, the laser linewidth was characterized using a delayed self-heterodyne measurement setup, using 22.5 km of optical fiber delay and an 80 MHz acousto-optic modulator. These measurements indicate a laser linewidth of 1 MHz. In conclusion, heterogeneous III-V/silicon DFB lasers with high optical confinement in the III-V laser mesa coupled to a silicon strip waveguide circuit were realized. The good device performance allows its use both for short-distance and long-distance optical communication. This demonstration paves the way for the realization of advanced III-V/silicon transmitter modules comprising III-V/silicon DFB lasers, silicon optical modulators and Ge photodetectors.

Support of the EU commission through the EU-project HELIOS.

References

1. S. Selvaraja, W. Bogaerts, P. Dumon, D. Van Thourhout, and R. Baets, IEEE J. Sel. Top. Quantum Electron. **16**, 316 (2010).
2. M. Watts, W. Zortman, D. Trotter, R. Young, and A. Lentine, Opt. Express **19**, 21989 (2011).
3. L. Vivien, J. Osmond, J. M. Fedeli, D. Marris-Morini, P. Crozat, J.-F. Damiencourt, E. Cassan, Y. Lecunff, and S. Laval, Opt. Express **17**, 6252 (2009).
4. R. E. Camacho-Aguilera, Y. Cai, N. Patel, J. T. Bessette, M. Romagnoli, L. C. Kimerling, and J. Michel, Opt. Express **20**, 11316 (2012).
5. G. Roelkens, L. Liu, D. Liang, R. Jones, A. Fang, B. Koch, and J. Bowers, Laser Photon. Rev. **4**, 751 (2010).
6. A. Fang, E. Lively, Y. Kuo, D. Liang, and J. E. Bowers, Opt. Express **16**, 4413 (2008).
7. S. Keyvaninia, G. Roelkens, D. Van Thourhout, C. Jany, M. Lamponi, A. Le Leipvre, F. Lelarge, D. Make, G. Duan, D. Bordel, and J. M. Fedeli, Opt. Express **21**, 2784 (2013).
8. S. Keyvaninia, S. Verstuyft, S. Pathak, F. Lelarge, G. H. Duan, D. Bordel, J. M. Fedeli, J.-M. Fedeli, T. De Vries, B. Smalbrugge, E. J. Geluk, J. Bolk, M. Smit, G. Roelkens, and D. Van Thourhout, Opt. Express **21**, 13675 (2013).
9. H. Park, M. Sysak, H. W. Chen, A. Fang, D. Liang, L. Liao, B. Koch, J. Bovington, Y. Tang, K. Wong, M. Jacob-Mitos, R. Jones, and J. Bowers, IEEE J. Sel. Top. Quantum Electron. **17**, 671 (2011).
10. S. Stankovic, R. Jones, M. N. Sysak, J. M. Heck, G. Roelkens, and D. Van Thourhout, IEEE Photon. Technol. Lett. **24**, 2155 (2012).
11. S. Keyvaninia, M. Muneeb, S. Stankovic, R. van Veldhoven, D. Van Thourhout, and G. Roelkens, Opt. Mater. Express **3**, 35 (2013).
12. M. Lamponi, S. Keyvaninia, C. Jany, F. Poingt, F. Lelarge, G. de Valicourt, G. Roelkens, D. Van Thourhout, S. Messaoudene, J.-M. Fedeli, and G. H. Duan, IEEE Photon. Technol. Lett. **24**, 76 (2012).